Results from a three-dimensional, nested biological-physical model of the California Current System and comparisons with statistics from satellite imagery

Thomas M. Powell,[1] Craig V. W. Lewis,[1] Enrique N. Curchitser,[2] Dale B. Haidvogel,[3] Albert J. Hermann,[4] and Elizabeth L. Dobbins[4]

Received 25 May 2004; revised 27 June 2005; accepted 11 August 2005; published 21 July 2006.

[1] A three-dimensional model of the California Current System (CCS) from 35°N to 48°N extending offshore to 134°W is coupled with a four-component trophic model. The model reproduces many conspicuous characteristics in the CCS, including: complex, filamentary, mesoscale surface features seen in the pigment and temperature from satellite imagery; wind-driven coastal upwelling at appropriate spatial and temporal scales; and the close correlation between prominent features seen in pigment and those in temperature observed by satellites (Abbott and Zion, 1985). Statistical estimates of the characteristic spatial scales of variability, as calculated from the coupled, nested model, agree with those previously estimated from satellite images (for both surface temperature and pigment (Denman and Abbott, 1988, 1994)). Model estimates of the characteristic temporal scales of variability, from decorrelation times, agree with those previously estimated from satellite images. Typical model decorrelation times lie between 2 and 4 days, in agreement with calculations from earlier sequences of (Coastal Zone Color Scanner (CZCS) and advanced very high resolution radiometer (AVHRR)) satellite images (Denman and Abbott, 1988, 1994).

Citation: Powell, T. P., C. V. W. Lewis, E. N. Curchitser, D. B. Haidvogel, A. J. Hermann, and E. L. Dobbins (2006), Results from a three-dimensional, nested biological-physical model of the California Current System and comparisons with statistics from satellite imagery, *J. Geophys. Res.*, *111*, C07018, doi:10.1029/2004JC002506.

1. Introduction

[2] The California Current System (CCS) forms the eastern boundary of the North Pacific Gyre, extending roughly from the southern tip of Vancouver Island to the southern end of Baja California and approximately 1000 km offshore. The West-Wind Drift, the northern portion of the North Pacific Gyre, delivers fluid to this eastern boundary current system. Surface flows in the CCS are equatorward, in the mean; these mean flows are termed the California Current. Also, a poleward-flowing, subsurface undercurrent, the California Undercurrent, is centered on the continental slope as a persistent feature from Baja California to Vancouver Island. In addition, the northward moving Davidson Current, a surface current inshore of 100 km from the coastline, flows during fall and winter months from Point Conception to Vancouver Island. These three currents, the California Current, the California Undercurrent, and the Davidson Current, compose the large-scale currents that make up the CCS. The region has been extensively studied, and the reader is referred to excellent reviews of the coastal oceanography of the CCS by *Hickey* [1979, 1998].

[3] Large-amplitude processes of an episodic nature also occur in the CCS, leading to smaller-scale features. These processes dominate records of both surface phenomena and sub-surface features. Coastal upwelling is one example, an important physical process in the CCS whose biological implications are large and well known [e.g., *Richards*, 1981; *Summerhayes et al.*, 1995]. For example, enhanced primary productivity commonly found inshore of a (coastal) upwelling front is the result of vertical motions bringing high concentrations of nutrients and a seed stock of large (>5 μm) photosynthesizing cells into a suitable, near-surface light environment [*Denman and Powell*, 1984]. Further, high nearshore concentrations of zooplankton can be maintained by a combination of upwelling and sinking. That is, zooplankton moving offshore in the surface layers sink (through diurnal vertical migration) into onshore-moving near-bottom fluid that is upwelled to the surface near the shore (see *Batchelder et al.* [2002] for a modeling investigation of this process). A second process involves the mesoscale filaments, or coastal jets, in this eastern boundary current system. Satellite imagery from the late 1970s [e.g., *Bernstein et al.*, 1977; *Traganza et al.*, 1980] showed that

[1]Department of Integrative Biology, University of California, Berkeley, Berkeley, California, USA.
[2]Division of Ocean and Climate Physics, Lamont-Doherty Earth Observatory, Palisades, New York, USA.
[3]Institute of Marine and Coastal Sciences, Rutgers University, New Brunswick, New Jersey, USA.
[4]Joint Institute for the Study of Atmosphere and Ocean (JISAO), University of Washington, Seattle, Washington, USA.

0148-0227/06/2004JC002506$09.00

high-velocity filaments, often with elaborate, mesoscale shapes ($\leq$100–200 km in size), were the dominant coastal features in both surface temperature and surface chlorophyll fields. *Abbott and Zion* [1985] demonstrated that the structures seen in images for surface temperature (from AVHRR imagery) were nearly identical to structures seen in surface chlorophyll (from CZCS) when the images were captured approximately synchronously. This close correspondence between surface temperature and chlorophyll (pigment) suggests the importance of physical phenomena to biological processes in this environment. Subsequent workers confirmed the role of the filaments and jets in a number of biologically critical processes: for example, (1) in the delivery of nutrients and resultant impact on primary productivity, phytoplankton biomass, and species composition [*Chavez et al.*, 1991]; (2) in the photosynthetic response to light in phytoplankton [*Hood et al.*, 1991]; (3) in the offshore transport of phytoplankton in a subducting jet [*Washburn et al.*, 1991]; (4) in the zooplankton community composition and pattern, which is not constant across a jet/filament [*Mackas et al.*, 1991]; (5) in egg production and lipid storage, and their relationship to food concentration in a jet [*Smith and Lane*, 1991]; and (6) in the genetic heterogeneity in a common copepod, *Metridia pacifica*; that is, there are two distinct population groups, one in eddies/jets, and the other offshore [*Bucklin*, 1991].

[4] Phenomena occurring on longer, interannual timescales can have important consequences for the California Current system [e.g., *Chavez et al.*, 2003]. Most of these phenomena are very large scale, affecting the entire North Pacific, even extending into equatorial waters. One such process is the El Niño–Southern Oscillation (ENSO), with a recurrence time of 2–7 years. ENSO effects have been studied extensively, especially during the last 2 decades (see *Chavez et al.* [2002] for a recent, comprehensive review of the topic). Another process is the Pacific Decadal Oscillation (PDO) [*Mantua et al.*, 1997; *Bond*, 2000] with a period that is believed to be 20–30 years. *Miller et al.* [2003] have recently reviewed important ecosystem effects generated by this phenomenon. Finally, anomalous events occur over large areas of the North Pacific that do not seem to be connected to any identifiable recurring process. For example, in 2002, much of the North Pacific was $\geq$1°C cooler than normal. This large-scale cooling is described by *Huyer* [2003]; observed physical and biological effects of this cooling were profound.

[5] These observations set the context for investigators attempting to model ecosystem features in the California Current System. First, the model must extend across a broad range of spatial scales. That is, much variability exists at modest to intermediate scales, as demonstrated by the extensive satellite studies of coastal features in the CCS. However, in addition, large-scale, even basin-scale, phenomena (ENSO, PDO, etc.) play a crucial role in understanding, and explaining, variability in the CCS. For example, ENSO impacts on temperature, salinity, etc., and thus stratification and vertical mixing, are well known in the CCS [*Chavez et al.*, 2002]. Substantial biological changes can be seen within 100 km of the shoreline. Thus the onset, growth, and decline of ENSO events, processes that occur on the scale of 4–6 months, may lead to changes in spatial pattern at modest scales (100–1000 km) in the CCS region. Accordingly, a satisfactory, comprehensive model must faithfully reproduce basin-scale phenomena over interannual timescales, and link these phenomena to the filamentous, eddying features found at substantially smaller scales (O(100 km)) and to coastal upwelling (at very least, the effects of large-scale features (e.g., differing wind fields) must enter models for smaller-scale phenomena, especially if one is interested in the relative importance of variance at different spatial scales, as we are in this work). Computational limitations will not presently allow a full three-dimensional (3-D) calculation that encompasses this fine horizontal resolution over the entire North Pacific with an appropriate number ($\sim$30) of levels in the vertical. One way around this difficulty is to "nest" (or embed) a fine-scale (high resolution) calculation within a coarser-scale (low resolution) calculation, passing information from the coarse to the fine. Both coarse- and fine-scale calculations can then be of manageable size. So long as one is careful concerning the details of information passing from large to small, this is a workable approach until greater computational resources become available. Second, the physical transports and the ecological processes must be modeled together. The nature of the problem at all spatial and temporal scales is a coupled one. In particular, knowledge of the physical transports is crucial to determining both the rates of change of ecological properties and their distribution in space. Moreover, the absorption of solar radiation in the water column, which affects heating, and thus stratification and vertical mixing, can, in turn, be affected by photosynthesizing organisms (i.e., phytoplankton; see equations (2) and (6)). Therefore, for the CCS, a satisfactory ecosystem model in this region should be a nested, coupled, 3-D biological-physical model.

[6] Model studies in the CCS region have a long history. A number of previous workers have produced coupled biological/physical models, though none have incorporated effects at the basin scale within a nested model framework, as described above. *Wroblewski* [1977] coupled a 2-D "slice" coastal circulation model (where the horizontal direction was onshore-offshore and vertical direction was depth [*Thompson*, 1978]) to a five-component ecosystem model. The five dynamic biological variables were: nitrate, ammonia, phytoplankton concentration, zooplankton concentration, and detritus. The model, designed for the Oregon coast, is a nitrogen-based model; all five components were specified in terms of nitrogen. In three papers, *Moisan and Hofman* [1996a, 1996b] and *Moisan et al.* [1996] developed a nine-component ecosystem model, including bio-optics, which the authors coupled to a 3-D circulation model that develops filaments in idealized bathymetry and coastal topography. The spatial relationship between the modeled filament structures and modeled regions of the high nutrient and high phytoplankton concentrations agree with general observations, i.e., the high-nutrient and high-phytoplankton regions lie onshore and in the core of the filaments.

[7] *Allen et al.* [1995] and *Federiuk and Allen* [1995] used a 2-D, onshore-offshore slice geometry with a substantially more complex model for the coastal circulation to explore in detail the response of modeled coastal upwelling to a variety of model configurations. The authors emphasized the need to incorporate realistic surface heat flux, initial density, and alongshore velocity distributions. *Allen and Newberger* [1996] used the same model to investigate

downwelling conditions, focusing on interesting downwelling frontal features. None of the three model studies above [*Allen et al.*, 1995; *Federiuk and Allen*, 1995; *Allen and Newberger*, 1996] incorporated an ecosystem model. Fully 3-D versions of the earlier model used by *Allen et al.* [1995] were further employed off the Oregon coast [*Blumberg and Mellor*, 1983; *Oke et al.*, 2002a, 2002b, 2002c; *Gan and Allen*, 2002a, 2002b; *Pullen and Allen*, 2001]. None of the *Pullen and Allen* [2001], *Gan and Allen* [2002a, 2002b], or *Oke et al.* [2002a, 2002b, 2002c] calculations included an ecosystem model.

[8] *Edwards et al.* [2000] and *Batchelder et al.* [2002] used simple ecological models (NPZ (Nutrient-Phytoplankton- Zooplankton), and an IBM (individual-based-model), respectively) in a 2-D slice geometry to explore how different biological parameterizations influence the spatial distribution of biota in idealized upwelling situations. *Edwards et al.* [2000] found that grazing terms which characterize microzooplankton led to substantially narrower zonal (cross-shelf) peaks in phytoplankton and zooplankton distributions than those produced by more conventional macrozooplankton grazing parameters. *Batchelder et al.* [2002] found that zooplankton diurnal vertical migration is necessary in order to retain zooplankton nearshore, where upwelling is most active and food resources highest. In the Oregon coast 2-D model geometry earlier studied by *Allen et al.* [1995] and *Federiuk and Allen* [1995], *Allen and Newberger* [1996] and *Spitz et al.* [2003] compared the behavior of biological quantities in three related ecosystem model structures: NPZ, NPZD (NPZ plus detritus, D), and NNPZD (two nutrients, plus P, Z, and D). Though *Spitz et al.* [2003] found differences in the spatial and temporal responses to coastal upwelling, the qualitative behavior seen in all three models was similar.

[9] *Marchesiello et al.* [2003] describe results from ROMS (Regional Ocean Modeling System), a 3-D, terrain-following model for the CCS. The authors present evidence for agreement between ROMS and the general features of the California Current. Other components of the CCS (standing eddies, cross-shore structures, seasonal currents, and mesoscale variability) also conform to the ROMS simulations. We employ the same 3-D circulation model, but in a different configuration; accordingly, some information on ROMS can be found below, but for further details, the reader is directed to *Marchesiello et al.* [2003].

[10] Satellite observations in the CCS region also provide important information for coupled biological-physical models. As noted above, *Abbott and Zion* [1985], studying simultaneous (or near simultaneous) AVHRR (temperature) and CZCS (chlorophyll pigment) images, found that the prominent features from one record are closely mirrored in the other. Extending this analysis, *Denman and Abbott* [1988, 1994] considered pairs of images from the same spatial location, but separated in time. They found that the spectral statistics (from 2-D, spatial, (fast) Fourier transforms] for individual images agreed closely with one another; that is, the variance spectrum falls as $|(\text{wavenumber})|^{-2}$. Moreover, using the coherence spectrum [cf. *Bendat and Piersol*, 1986; *Diggle*, 1990], Denman and Abbott also found that the correlation within a wave number band between pairs of images falls with increasing separation time. A characteristic decorrelation time was 2–4 days. This was true of pigment-pigment, temperature-temperature, and pigment-temperature decorrelations. That the pattern decorrelation times are identical (or very close) is an indication that the pigment patterns are under physical control. The satellite studies of Denman and Abbott provide valuable observational information about the dominant temporal and spatial scales of variability in the CCS. That is, the dominant spatial scales (where the largest spatial variance occurs) are the largest spatial scales, up to approximately 100 km (the upper limit due to sampling protocols); temporal coherence falls off quickly beyond lags of 2–4 days.

[11] In this study we ask whether nested-model systems coupled with a simple ecological model (i.e., a high-resolution model of the CCS embedded within a coarse-resolution, basin-scale model for the North Pacific) reproduce the prominent California Current features? Most importantly, can the coupled, nested model reproduce the space and timescales of variability for both physical and biological quantities as derived from satellite observations of this eastern boundary current region?

2. Methods

[12] We describe here the two elements of our analysis. The first is a 3-D circulation model nested within a set of larger models, with a fully coupled biological model. The second is the spectral method used by *Denman and Abbott* [1988, 1994] to determine if scales of variability in model temperature and phytoplankton distributions are consistent with the Denman and Abbott results from satellite images.

2.1. Circulation Model

[13] The circulation model used in this article is the Regional Ocean Modeling System (ROMS) version 2.0 (development is described by *Song and Haidvogel* [1994], *Haidvogel and Beckmann* [1999], *Haidvogel et al.* [2000], *Marchesiello et al.* [2003], and *Shchepetkin and McWilliams* [2003]. ROMS is a hydrostatic primitive equation model which uses a terrain-following, orthogonal finite difference grid that can be stretched and curved to increase resolution in regions of interest and masked for land regions.

[14] The grid extends from approximately Neah Bay, Washington, in the north, to Point Conception, California, in the south, extending offshore about 1000 km to longitude 134°W. The vertical profile is resolved by 30 sigma levels concentrated near the surface; this provides resolution of 0.7 m nearshore. Off the shelf, with a 5000-m bottom depth, the vertical resolution ranged from 15 m at the surface to 450 m at the bottom. Bathymetry is supplied by ETOPO5 [*National Geophysical Data Center*, 1988].

[15] Surface momentum transfer and mixing profiles were calculated using the order 2.5 turbulence closure model (MY2.5) of *Mellor and Yamada* [1982]. The MY2.5 model was found to provide mixing profiles which varied smoothly in time and space [*Durski et al.*, 2004].

2.2. Nested Boundary Conditions

[16] Initial conditions and boundary forcing for this model were drawn from a nested set of larger-scale models described by *Curchitser et al.* [2005]. The boundary and

initial values of temperature, salinity, velocity and sea-surface height for the CCS simulation are drawn from a simulation of the Northeast Pacific (NEP) at 10-km horizontal resolution. This domain was similarly driven by a model of the entire North Pacific (NPac) at 40-km resolution (full domain shown in Figure 1). Other similar nested modeling studies include those of *Hermann et al.* [2002] and *Harding et al.* [2002].

[17] The NPac domain is initialized with climatological temperature and salinity fields [*Levitus and Boyer*, 1994; *Levitus et al.*, 1994]; the first 10 modeled years were forced by COADS buoyancy fluxes [*Woodruff et al.*, 1998] and NCEP [*Kistler et al.*, 2001] climatological winds. The NPac domain was then run for 10 years using daily specified 1990 to 2003 wind and atmospheric data from the NCEP Reanalysis Project [*Kistler et al.*, 2001]; surface heat fluxes and surface stress were calculated using the bulk-flux formulation of *Fairall et al.* [1996a, 1996b]. The NPac model state at the beginning of hindcast year 1996 was interpolated onto the NEP grid to initialize model runs for that intermediate-scale domain. The NEP grid was run for the 1996–2003 period using the same daily forcing as the NPac grid.

[18] For the 3-D variables (U, V, and tracers) we use the radiation boundary condition with adaptive nudging described by *Marchesiello et al.* [2001, 2003]. At all open boundaries, the model uses a *Chapman* [1985] boundary condition for the free surface, with *Flather* [1976] boundary conditions on the 2-D momentum and adaptive nudging and radiation on 3-D momentum and tracers (for a more complete description, see *Marchesiello et al.* [2001]). Thus processes and features resolved at larger scales by the NPac model are passed in through the boundaries of the NEP grid, while the interior dynamics of the NEP grid can evolve finer scales. The interior of the NEP domain responds to the same forcing as the NPac domain, though with better resolution of the spatial and temporal scales.

[19] The same type of nesting (termed ''one-way nesting'') occurs between the NEP grid (10-km resolution) and the CCS grid (3-km resolution). For the simulations discussed here, the model is initialized with interpolated results from the NEP grid on 1 January 2000. The model is then forced with daily meteorological data from year 2000 in the same fashion as the preceding NPac and NEP models.

2.3. Biological Model

[20] Biological dynamics are modeled using a four-element, nitrogen-based trophic model. Total nitrogen at any given point is partitioned between dissolved nitrogen (N), particulate nitrogen (Detritus: D), phototrophic phytoplankton (P), and herbivorous zooplankton (Z). The four dynamical equations ((1)–(4) for N, P, Z, and D) have the same general form. The left-hand side of each equation contains two terms: a local time derivative (e.g., ∂N/∂t, ∂P/∂t), and an advective term (e.g., $\mathbf{u} \cdot \nabla$N, $\mathbf{u} \cdot \nabla$P). The right-hand side of each equation has several terms, but the last term in each equation has the form [$\partial/\partial z(k_v \partial N/\partial z)$, $\partial/\partial z(k_v \partial P/\partial z)$, etc.], which are the vertical transport, or vertical mixing, terms. The remaining terms on the right-hand-side of equations (1)–(4), exclusive of the vertical mixing terms, represent the biological dynamics (including the sinking term in equation (4), $w_d \partial D/\partial z$, within biological dynamics).

$$\frac{\partial N}{\partial t} + \mathbf{u} \cdot \nabla N = \delta D + \gamma_n GZ - UP + \frac{\partial}{\partial z}\left(k_v \frac{\partial N}{\partial z}\right), \quad (1)$$

$$\frac{\partial P}{\partial t} + \mathbf{u} \cdot \nabla P = UP - GZ - \sigma_d P + \frac{\partial}{\partial z}\left(k_v \frac{\partial P}{\partial z}\right), \quad (2)$$

$$\frac{\partial Z}{\partial t} + \mathbf{u} \cdot \nabla Z = (1 - \gamma_n)GZ - \zeta_d Z + \frac{\partial}{\partial z}\left(k_v \frac{\partial Z}{\partial z}\right), \quad (3)$$

$$\frac{\partial D}{\partial t} + \mathbf{u} \cdot \nabla D = \sigma_d P + \zeta_d Z - \delta D + w_d \frac{\partial D}{\partial z} + \frac{\partial}{\partial z}\left(k_v \frac{\partial D}{\partial z}\right), \quad (4)$$

$$G = R_m\left(1 - e^{-\Lambda P}\right), \quad (5)$$

$$I = I_0 \exp\left(k_z z + k_p \int_0^z P(z')dz'\right), \quad (6)$$

$$U = \frac{V_m N}{k_N + N} \frac{\alpha I}{\sqrt{V_m^2 + \alpha^2 I^2}}. \quad (7)$$

[21] The NPZD model (equations equations (1)–(7)), is identical to that of *Spitz et al.* [2003] (and, with minor differences (for the saturating forms for (1) the photosynthetic response to light, and (2) the grazing response of zooplankton to phytoplankton) to the NPZD model used by *Denman and Pena* [1999]). Major processes included in the model are photosynthetic growth and uptake of nitrogen by phytoplankton (U), grazing on phytoplankton by zooplankton (G), mortality of both types of plankton (σ_d for phytoplankton, and ζ_d for zooplankton), and sinking (w_d) and remineralization (δ) of detritus. For simplicity (following *Spitz et al.* [2003]), surface light levels are assumed constant with time; available light at depth z is calculated assuming exponential attenuation by (1) seawater (k_z), and (2) phytoplankton (k_p), with the extinction coefficient for phytoplankton being proportional to the average phytoplankton density between the surface and depth z. A Michaelis-Menten curve was used to describe the change in uptake rate as a function of nitrate concentration (U). Grazing of zooplankton on phytoplankton is parameterized using the Ivlev function (G), with some proportion (γ_n) of the consumed phytoplankton being lost directly to the nitrate pool as a function of ''sloppy feeding'' and metabolic processes. Mortality and remineralization terms are linear functions of concentration; dead plankton becomes detritus (σ_d, ζ_d), while detritus is remineralized to become dissolved nitrogen (δ). None of the biological processes here are temperature dependent.

[22] The parameters used in the model are listed in Table 1; they are identical to those used by *Spitz et al.*

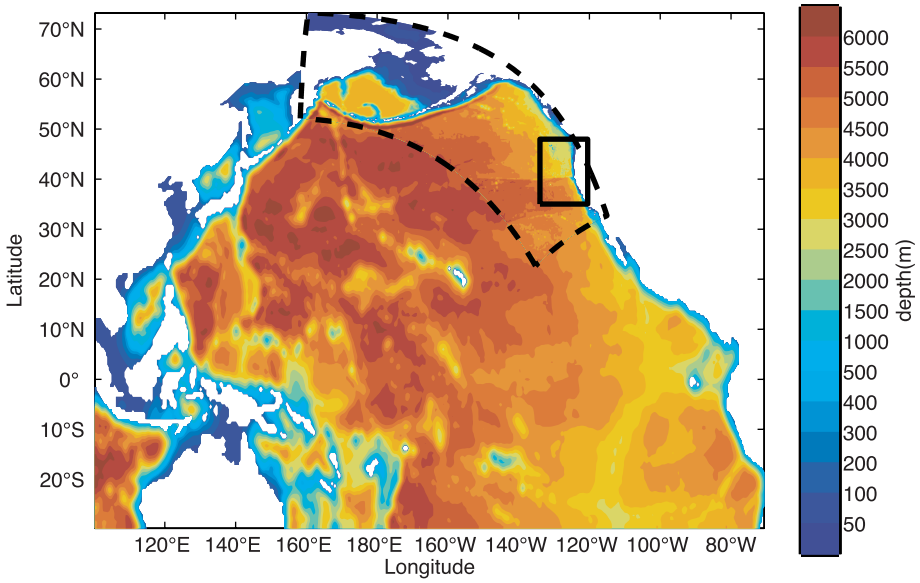

Figure 1. Northern Pacific (NPac) model bathymetry, with inserted finer-resolution northeast Pacific (NEP, dashed line), and California Current System (CCS, solid line) model domains (see section 2.2).

[2003]. With few exceptions, the parameters are also identical to those used by *Wroblewski* [1977] and calibrated for the upwelling region off Oregon (Wroblewski's five component model contained two dissolved nitrogen components, ammonia and nitrate, but was otherwise identical to the NPZD model analyzed here). It was not our purpose to explore the sensitivity of our results to the specific parameters that were selected for our calculations. Moreover, in 1-D and 2-D calculations, *Spitz et al.* [2003] and *Newberger et al.* [2003] performed a thorough, careful analysis of the dependence of results from this model (and two closely related models, as discussed in section 1) on model parameters. In summary, the NPZD model, including the selection of model parameters, has a long history of use in the CCS region and represents a good choice for the study reported here.

[23] The model in the CCS area (see Figure 1) was initialized with uniform fields in N, P, Z, and D (respectively, 17, 1, and 1 μM). These non-equilibrium initial conditions cause the model to oscillate and bloom for the first 2 months (~60 days), but the transient behavior declines and is not seen after 120 days (see Figures 2 and 3 for the early period, and Figures 4 and 5 for the later calculation times).

[24] No biological model calculations are performed in the intermediate NEP region (or the basin-scale NPac region; see Figure 1). Accordingly, values for N, P, Z, and D on the boundary of the CCS region are held constant at their initial values.

[25] Coupling of the biological and physical models is straightforward. The time step of the physical model is more than sufficient to resolve biological processes, and both models were run as one. N, P, Z, and D are advected and diffused synchronously with temperature and salinity fields, by identical algorithms. The high-order advection schemes used are conservative but not positive-definite. A conservative filter is applied to prevent biological quantities from taking negative values; when negative values are detected, nitrogen was drawn from the most abundant pool to supplement the negative pools to a lower limit of 10^{-6}mmol N m^{-3}. These simulations are performed on 64 processors (either eight 8-processor nodes or two 32-processor nodes) of the massively parallel computer, "Bluesky," at the National Center for Atmospheric Research. Monthly simulations could usually be performed in 6 hours.

2.4. Comparison to Satellite Data

[26] Calculation of autospectra and coherence spectra were performed with MATLAB (Mathworks Corporation, Natick, Massachusetts), closely following methods clearly described by *Denman and Abbott* [1988]. The model spatial resolution is lower than the resolution of the satellite images studied by *Denman and Abbott* [1988, 1994], but no problems exist in model information analogous to the spatial or temporal gaps caused by clouds, satellite timing, or field-of-view. To summarize, this work better addresses temporal lags but does not resolve processes at the finest spatial scales discussed by *Denman and Abbott* [1988, 1994].

Table 1. Parameter Values

Parameter Name	Symbol	Value	Dimension
Light extinction coefficient	k_z	0.067	m^{-1}
Self-shading coefficient	k_p	0.0095	m^2 mmol-N^{-1}
Initial slope of P-I curve	α	0.025	m^2 W^{-1}
Surface irradiance	I_O	158.075	W m^{-2}
Nitrate uptake rate	V_m	1.5	d^{-1}
Uptake half saturation	k_N	1.0	mmol-N m^{-3}
Phytoplankton senescence	σ_d	0.1	d^{-1}
Zooplankton grazing rate	R_m	0.52	d^{-1}
Ivlev constant	Λ	0.06	m^3 mmol-N^{-1}
Excretion efficiency	γ_n	0.3	
Zooplankton mortality	ζ_d	0.145	d^{-1}
Remineralization	δ	1.03	d^{-1}
Detrital sinking rate	w_d	8.0	m d^{-1}

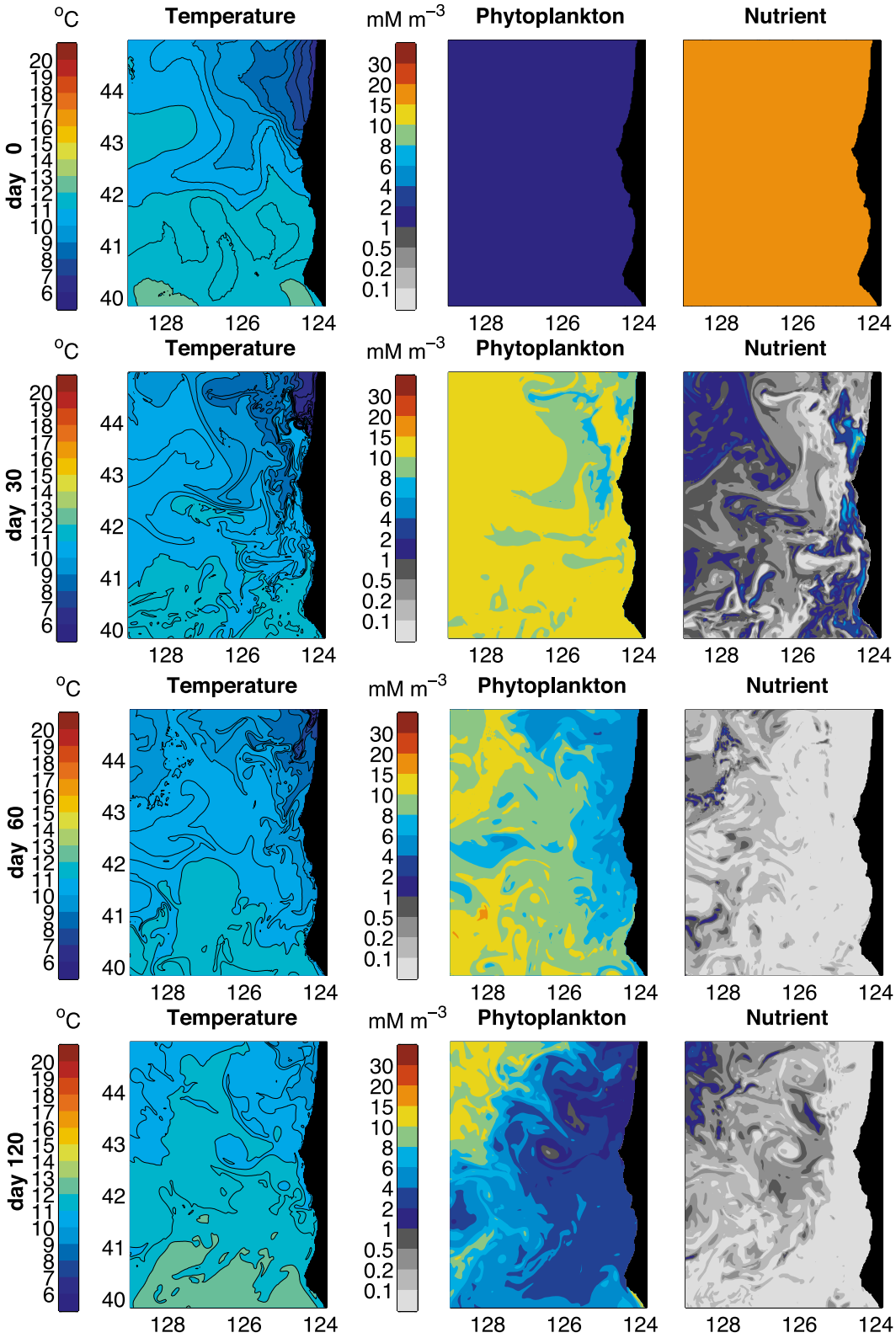

Figure 2. Surface expression of temperature, T (lines every 0.5°C), phytoplankton, P, and dissolved nitrogen, N ("Nutrient"), calculated at days 0 (initial conditions), 30, 60, and 120.

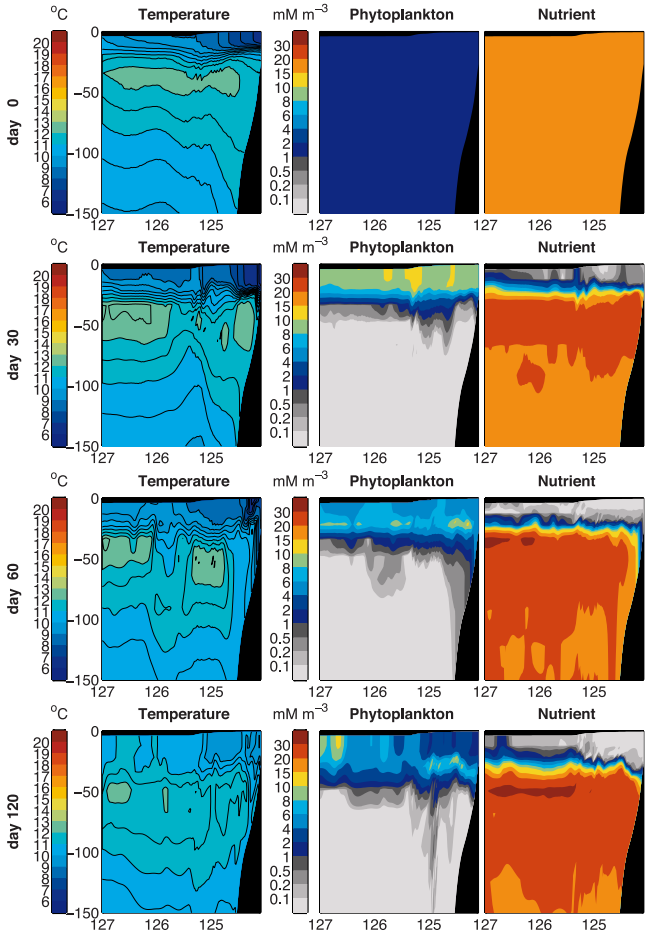

Figure 3. Vertical section for temperature, phytoplankton, and dissolved nitrogen offshore of Newport, Oregon, calculated at days 0 (initial conditions), 30, 60, and 120 (depths in meters, distance in degrees longitude).

[27] Spectral calculations focused on a square window extending from latitude 40°44′N to 44°8′N and longitude 129°W to 124°37′W (see Figure 6). This selection excludes the shelf regions from the analysis, which was also the choice made by *Denman and Abbott* [1988, 1994]. The spectral estimates were calculated on data from days 180 to 270 (see Figures 7, 8, and 9). Our calculations use the surface layer of the modeled phytoplankton and temperature fields as analogs to the CZCS and AVHRR data studied by *Denman and Abbott* [1988, 1994]. The 2-D data were detrended and median-filtered, and a 10% cosine taper was applied.

[28] Coherence, cospectra, and autospectra were then calculated from the 2-D FFT of the smoothed data. These were reduced to 1-D autospectra and 1-D coherence spectra by azimuthal summation over concentric rings in (2-D) wave number space; that is, the width of the concentric rings corresponded to the wave number bands of interest. Our coherence analysis focused on wavelengths of 25–50 km and 50–100 km. The reader is directed to the thorough discussions by *Denman and Abbott* [1988, 1994] regarding the algorithms that they used (and that were followed closely in the study we report here).

3. Results

[29] Analysis of the model results focuses on the general, qualitative nature of the calculated quantities, the spectral statistics of the temperature and phytoplankton distributions, and the lagged coherence between the temperature and phytoplankton patterns.

3.1. Representative Calculations

[30] Figures 2, 3, 4, and 5 illustrate the temperature and biological response within the GLOBEC study region, extending approximately from Newport, Oregon, to Cape Mendocino, California (solid box, CCS, Figure 6). As noted above, the initial conditions are interpolated from NEP results on 1 January 2000 onto CCS grid points. Boundary conditions are evaluated on the CCS boundaries from quantities calculated on the larger-scale NEP grid (see Figure 1). In this first section we emphasize the qualitative characteristics of calculated features. The following two sections 3.2 and 3.3 address the quantitative analysis of the spatial and temporal scales in the model.

[31] Figures 2–5 indicate that the circulation and tracer fields during the first 120 days may be influenced by the initial conditions, especially during the first 60 days. Thus it is appropriate to review our investigations of the "spin-up" characteristics of the nested model. First, "the physics" is adequately "spun up." As noted above, the largest-scale model (on the NPac grid, see Figure 1) is initialized with climatological temperature and salinity fields, and run for ten years with climatological winds and fluxes. Then, also noted above, the model is run from 1990 to 2003 with NCEP Reanalysis winds and calculated fluxes. At the next stage, the large-scale (NPac) results for January 1996 are interpolated onto the intermediate-scale (NEP) grid points for initial and boundary conditions, and the model is run on the intermediate scale from 1996 to 2003 with the same forcing as the large-scale model. Finally, it is these intermediate-scale model results that provide the initial and boundary conditions (see previous paragraph) for the (highest resolution) CCS model starting on 1 January 2000. Because the large-scale (NPac) model is spun up for a decade, and the intermediate-scale (NEP) model for 4 years, we are confident that "the physics" is adequately spun up. Second, we are also confident that beyond 120 days "the biology" is also adequately spun up. Though we present no results, we have run the NPZD model over 1000 times in various 0-D, 1-D, and 2-D configurations. In all cases, after 120 days the transient impact of initial conditions that are far from equilibrium is negligible. Finally, in the results from our simulation for later periods, Figures 4 and 5, days 180–240, there is no evidence of the transient behavior dominated by initial conditions.

[32] The initial stages of the calculations (Figures 2 and 3) show three dominant features. First, there is a transient adjustment away from non-equilibrium initial conditions, as expected. The initial, spatially uniform biological conditions are rapidly altered; extensive surface nitrogen is quickly taken up by phytoplankton, transferred to zooplankton, and then exported beneath the surface layer. There, high remi-

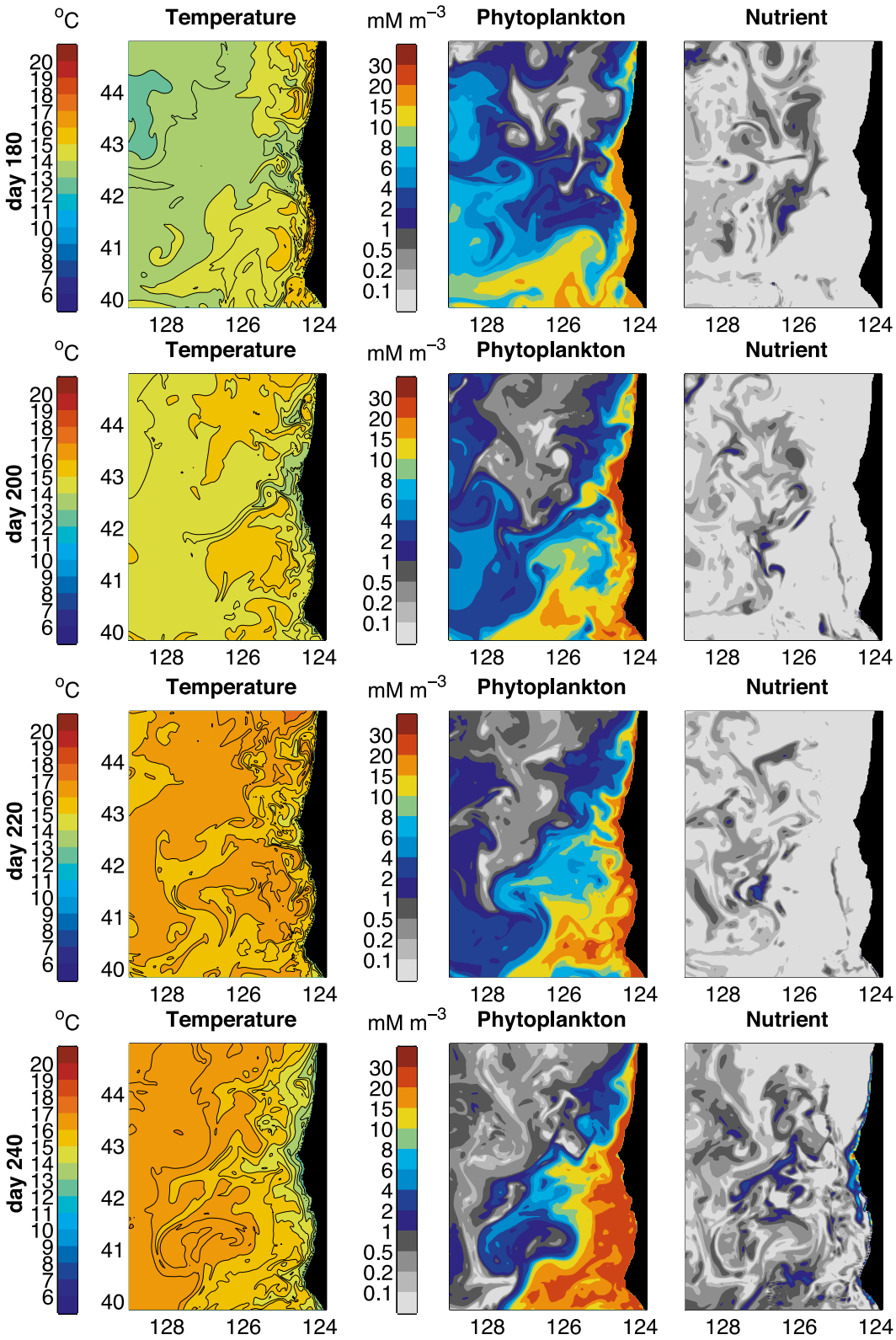

Figure 4. Surface expression of temperature, phytoplankton, and dissolved nitrogen calculated at days 180, 200, 220, and 240.

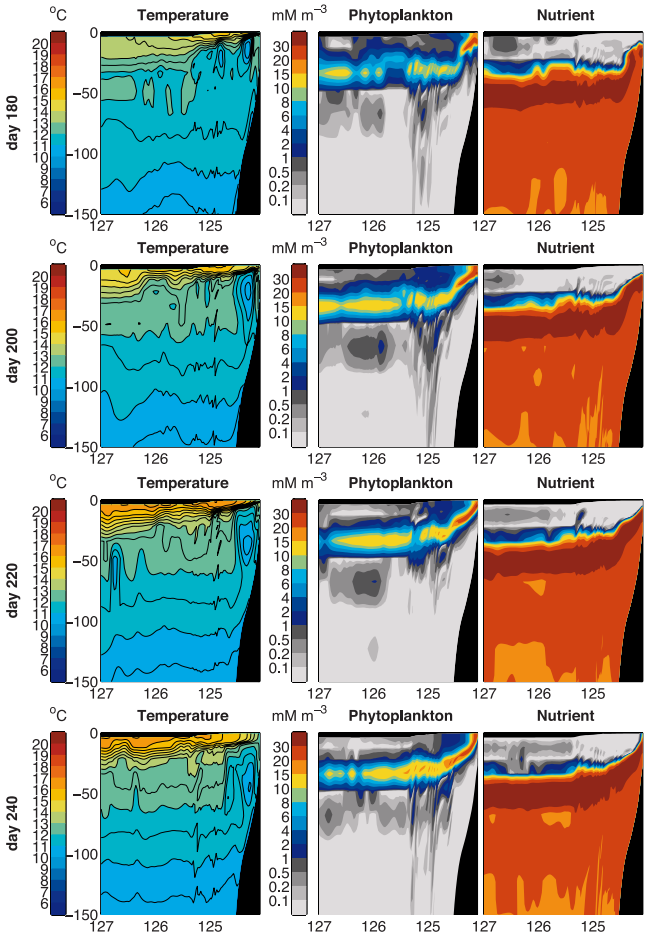

Figure 5. Vertical section for temperature, phytoplankton, and dissolved nitrogen offshore of Newport, Oregon, calculated at days 180, 200, 220, and 240 (depths in meters, distance in degrees longitude).

neralization rates result in high subsurface nutrient concentrations (see Figure 3). Second, fine-scale variability evolves from larger-scale (or even uniform) pattern. The NEP model from which the initial physical conditions were drawn does not resolve the smallest spatial scales of variability, but features at the finer scales resolved by the CCS grid develop quickly. The initial, smooth distributions of temperature and uniform distributions of biological properties (Figure 2, row 1) give way to much finer scales of variability (Figure 2, rows 2 and 3). Third, nearly identical features in "physical" and "biological" quantities develop (as in work by *Abbott and Zion* [1985]). During the first 4 months (Figure 2), the surface temperature, phytoplankton, and nitrate fields converge until features present in the physical fields are consistently mirrored in the biological fields. For example, on day 120 (Figure 2, row 4) an eddy and filament combination around 43°N, 126°W is captured as a cold eddy containing phytoplankton poor water. We caution the reader that early in the calculation period (especially for times before day 60) the results may be convolved with transient model response. However, the three qualitative characteristics of the California Current System, noted above, emerge by day 120.

[33] In the period represented by Figures 4 and 5, days 180–240, the transient response to initial conditions has died out and been replaced by the time-dependent response to surface and boundary forcing (see Figure 4). Coastal upwelling is a dominant feature, though the surface expressions of the upwelling-induced phytoplankton bloom extends only a few tens of kilometers offshore in the northern portion of the modeled area (see Figure 5). Surface warming begins to be evident near day 120 (Figures 2 and 3, row 4) and continues throughout the summer season (Figure 5), with the pycnocline appearing at approximately the proper depth (between 30 and 50 m [*Hickey*, 1998]) for the time of year. Prominent features are similar in nature to those commonly observed in satellite images. For example, an eddy, warm filament, and front extending WSW off Heceta Head (42°N) on day 200 (Figure 4, row 2, 125°W–127°W, 42°N) is nearly coincident with a plume of phytoplankton-enriched water in the same region.

[34] During the upwelling period, it is common for peak upwelling and eddy formation to occur south of Heceta Head (42°N), peaking off the California Coast [*Hickey*, 1998]. Examination of all model results during this period clearly show a marked transition at Heceta Head (Figure 4). The northern coast of Oregon has fewer, offshore large-scale surface features, while the coast south of Heceta Head is the base of an extensive group of filaments and jets extending well offshore. We note a commonly found upwelling structure, a dissolved nitrogen maximum at Heceta Head, on day 240 when dissolved nitrogen upwells in response to strong wind forcing during that period. The phytoplankton distributions in that region are slightly

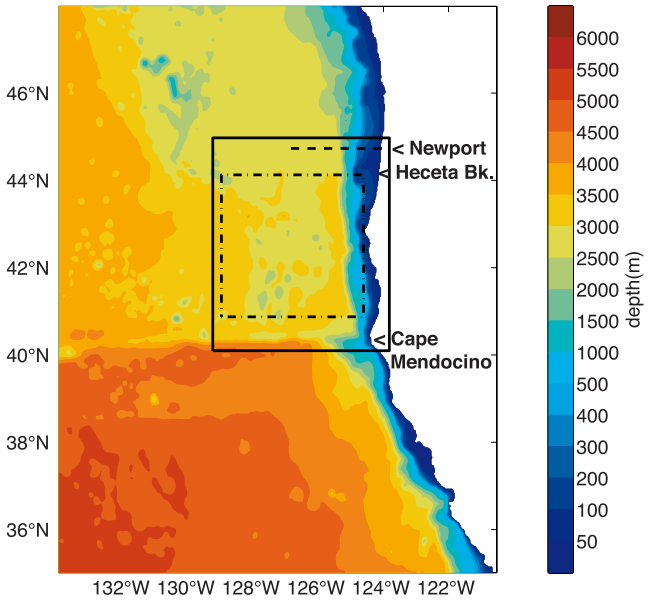

Figure 6. CCS Model bathymetry and extent. The area of interest for calculation of spectral quantities is indicated by the inner dash-dotted box; the area shown in Figures 2 and 4 is denoted by the outer solid box; the vertical section off of Newport, Oregon (~44.7°N), shown in Figures 3 and 5, is depicted by a dashed line.

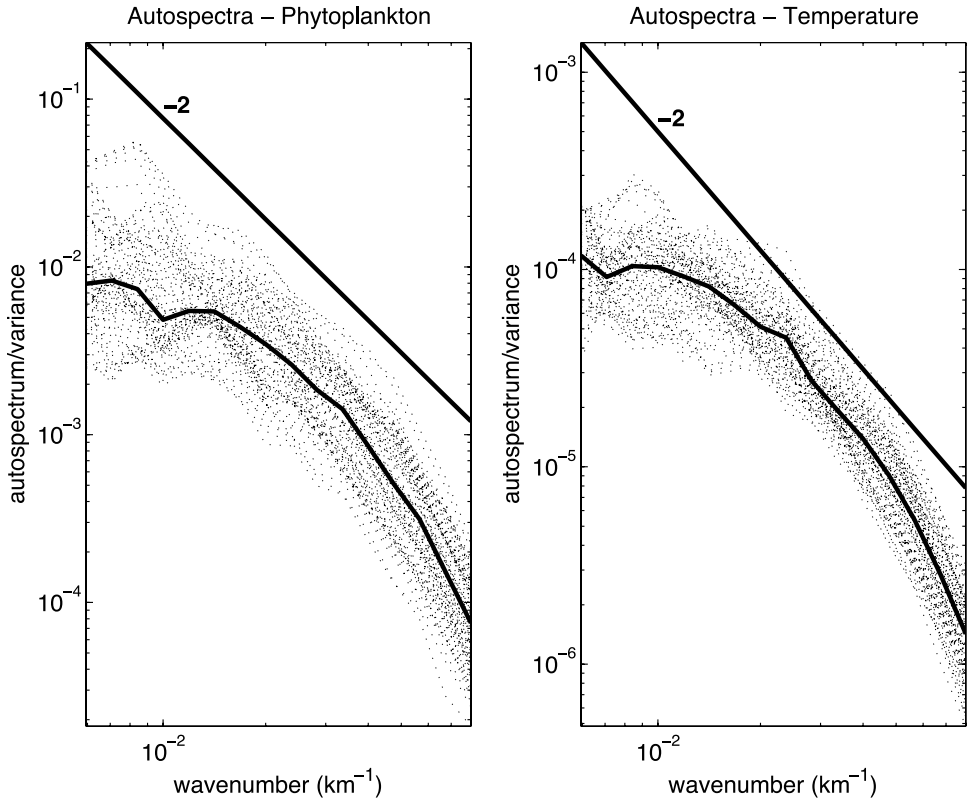

Figure 7. Autospectra for temperature and phytoplankton surface distributions, with the median shown by thick line. A line of −2 slope is added for reference. Data are calculated from daily averaged surface fields for model days 180–270.

reduced, not having had time to respond and bloom in the newly upwelled water.

3.2. Autospectral (2-D) Calculations

[35] The distribution of variability as a function of spatial scale, i.e., spatial pattern, spatial heterogeneity, or patchiness, has been noted as an important element of marine habitats for a half-century (recent references include *Denman and Dower* [2001] and *Martin* [2003]). A common measure of this distribution is the spectrum (or autospectrum) of a spatially varying biological, or physical, quantity. *Denman and Abbott* [1988, 1994] observed that the autospectra of both surface temperature and pigment are proportional to [wave number]$^{-2}$ (i.e., a plot of log(autospectra/variance) versus log(wave number) is a straight line with slope −2). Their calculations, based on CZCS and AVHRR imagery, were focused on several regions off the Oregon and California coasts. A similar analysis of our modeled surface temperature and pigment distributions in the same wave number band is consistent with the −2 slope (Figure 7), but the agreement is less compelling because there is more curvature in our autospectra than in the Denman/Abbott calculated quantities. That is, in the center of the wave number band our autospectra are proportional to [wave number]$^{-2}$ (Figure 7), but the curves are flatter at low wave numbers, and steeper at high wave numbers, than [wave number]$^{-2}$. The reason for the disagreement at high wave numbers is in part due to the lower resolution (3 km) of our model compared to the CZCS data resolution (1 km) [*Denman and Abbott*, 1988, 1994]. We note that at the smallest wave numbers (longest wavelengths), the slope of our autospectra does decrease, similar to that seen in the autospectra estimated by Denman and Abbott.

3.3. Coherence Spectrum Results

[36] An estimate of the squared coherence (as a function of wave number) between two records, separated in time, is a measure of the correlation between the two (within the wave number band, spatial scale, of interest). Such measures of correlation made for several time separations allow the investigator to estimate the duration for the correlation to shrink to insignificance, i.e., a decorrelation time. The squared coherence between temporally lagged temperature distributions and phytoplankton distributions are instructive because they allow one to make and compare estimates for characteristic decorrelation times for temperature (a ''physical'' quantity) and phytoplankton (a ''biological'' quantity). Such decorrelation times give one important information about how long to expect biological (and physical) features to persist within a given habitat. They may also allow one to make a first determination whether a biological response to a physical anomaly might be large or small. For example, an anomalously high nutrient concentration in a parcel of fluid that does not persist for long in a habitat (i.e., short decorrelation time), may not be in that habitat for a sufficient period to allow slowly growing plankton (perhaps dinoflagellates) to respond to the high-nutrient conditions.

[37] Comparing modeled temperature distributions to themselves (Figure 8) shows a coherence of 1.0 at lag 0, dropping to 0.03 within about 5 days at spatial scales

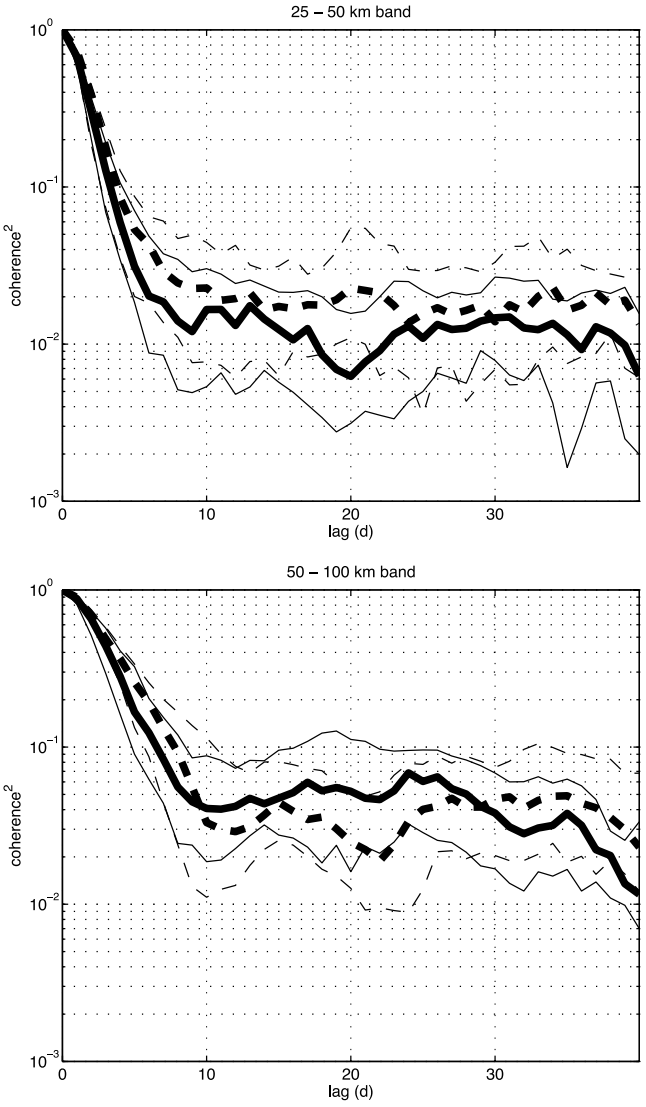

Figure 8. Squared coherence of time-lagged surface temperature (solid lines) and phytoplankton (dashed lines) distributions in two wave number bands: (top) 25–50 km and (bottom) 50–100 km, for lags of 0 to 40 days. Data were taken from model fields for days 180–270. Shown are median (thick lines) and 25th and 75th percentile lines.

between 25 and 50 km, and 0.04 within 10 days at spatial scales between 50 and 100 km; this is consistent with decay timescales of approximately 2 and 3 days, respectively. For lags greater than 20 days, squared coherence between lagged temperature fields at 25–50 km remains around 0.01, and at scales of 50–100 km stays near 0.02. The results for the squared coherence for modeled phytoplankton distributions compared to themselves do not differ statistically from the results for temperature (see Figure 8). These two results, for temperature and phytoplankton squared coherence, are nearly indistinguishable from those shown by *Denman and Abbott* [1994] as calculated from satellite imagery for an area containing a filament [*Denman and Abbott*, 1994, Figure 3]. The equality between temperature and phytoplankton decorrelation times (in both model and observations) is suggestive of the control which physical processes exert on biological patterns, as measured by indicators of phytoplankton concentration.

[38] The squared cross-coherence between temperature and phytoplankton may be even more instructive; it gives evidence for the degree of simultaneous evolution of spatial patterns in both quantities (in the wave number band(s) of interest). Though the separate quantities shown in Figure 8 may decorrelate at the same rate, one quantity could decorrelate from the other in very different fashion, for example, at different rates. Figure 9 shows the squared cross-coherence between modeled temperature and modeled phytoplankton for various time separations (lags). Note that

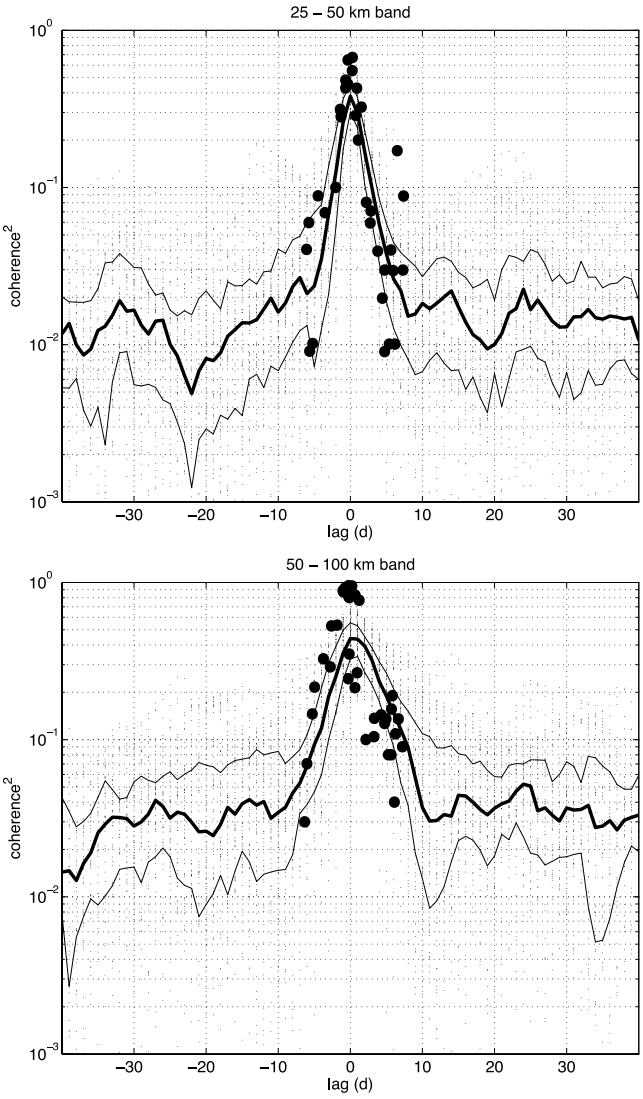

Figure 9. Squared coherence of time-lagged temperature and phytoplankton surface distributions in two wave number bands: (top) 25–50 km and (bottom) 50–100 km, for lags of 0 to 40 days. Data were taken from model fields for days 180–270. Shown are median (thick line) and 25th and 75th percentile lines. Solid circles represent data from *Denman and Abbott* [1994] for the squared coherence calculated for an area in the CCS containing a filament seen in satellite images for temperature and phytoplankton pigment.

the highest coherence occurs at zero lag in both wave number bands; lag zero squared cross-coherence between modeled temperature and phytoplankton is approximately 0.38 in the 25–50 km band, and 0.44 at 50–100 km scales (Figure 9). Background levels are similar to those for the temperature/temperature comparisons (0.02 at 25–50 km and 0.03 at 50–100 km). Decay timescales, estimated from the temperature/phytoplankton squared coherence, are approximately 2 days in the 25–50 km band, and 4 days for the 50–100 km scales, similar to the results for the temperature/temperature and phytoplankton/phytoplankton decorrelation times: 2 and 3 days, respectively. Note that at the larger spatial scales (50–100 km), the squared coherence between temperature and phytoplankton at a lag of 1 day is almost as high as the squared coherence at lag 0; this implies that the phytoplankton response may be slightly lagging the temperature variation. One might interpret this behavior in terms of upwelling phenomena; that is, the phytoplankton may need a day, or so, to take advantage of (i.e., grow in response to) upwelled nutrients in cooler waters. Also plotted on Figure 9 are the points derived by *Denman and Abbott* [1994] for the squared cross-coherence between temperature and phytoplankton obtained with satellite images from an area containing a filament [*Denman and Abbott*, 1994, Figure 3]. The Denman/Abbott points cluster around the model-derived squared cross-coherences; and most points lie within the 75th to 25th percentile envelope surrounding the model estimates. At zero lag the model-generated squared cross-coherences are lower than the values derived from satellite imagery, a point to which we return in the next section. Nonetheless, the peak in squared cross-coherence at zero lag between phytoplankton and temperature at both large and intermediate scales argues for the simultaneous evolution of the physical and biological patterns (as measured by phytoplankton and temperature). Moreover, the correspondence between the decorrelation times generated via squared cross-coherences from satellite observations and model calculations is a strong argument that the coupled biological/physical model is capturing the correct timescales, as observed in the CCS.

4. Discussion and Conclusion

[39] The results from our coupled biological-physical model are in qualitative agreement with the general characteristics of the California Current System (see section 3.1). The seasonal transitions and upwelling blooms common to the CCS region are captured by a simple model (NPZD coupled to an appropriate circulation and transport model) which focuses on the photosynthetic response of upwelled dissolved nitrogen to light. Nesting the CCS model within the larger-scale models (NPac, NEP) provides a conceptually simple and attractive method of delivering larger-scale forcing to the CCS boundaries. The coupled biological/physical model also reproduces the variability associated with finer-scale structures in which physical transports are closely linked to biological features. This close linkage between biological and physical features has long been known as an essential aspect of the CCS [e.g., *Abbott and Zion*, 1985]. It must be strongly emphasized that coupling to a "good" circulation/transport model that can resolve the finer-scale features is crucial. Our results confirm those of previous studies that ROMS (the model used in this and other studies [*Marchesiello et al.*, 2003]) does represent mesoscale features and processes with the spatial and temporal scales that are consistent with current synoptic observations. An important next step in comparing this model (and other coupled models) with observations will be to determine whether the magnitude and timing of evolving physical/biological features can be reproduced by the model(s), though it is likely that data assimilation will be necessary to accomplish this task successfully [*Oke et al.*, 2002c].

[40] The spatial and temporal scales of variability for temperature and phytoplankton distributions in this California Current System model are consistent with satellite-observed spatial and temporal scales in the same region. The autospectra plots (Figure 7) indicate that over a moderate region in wave number space the model spectra match the -2 slope calculated from satellite images by *Denman and Abbott* [1988, 1994], though there is more curvature in our spectra than the nearly straight lines (on a log-log plot) reported by Denman and Abbott. Coarser spatial resolution in the model ($\sim$3 km versus $\sim$1 km for the satellite imagery) may be the cause of the disagreement at high wave number. At low wave numbers (large spatial scales) the Denman and Abbott autospectra are beginning to "flatten" and "turn over" below the line with -2 slope, which is the shape we observe. In summary, for this region the model-generated autospectra resemble those derived from satellite imagery, which implies that the variance is distributed over spatial scales in approximately the same fashion. Hence, noting the caveats above, the characteristic spatial scales of the model calculations approximately agree with those observed from satellites.

[41] Turning to temporal scales, the squared coherence and cross-coherence plots generated by the model agree closely with those calculated from satellite images by *Denman and Abbott* [1988, 1994] (see Figure 8 and, especially, Figure 9). The decay of coherence happens more slowly at larger scales for both satellite and model, with most of the decay taking place in the first 10 days for larger scales and within 5 days at the smaller spatial scales; again, this is in accord with Denman and Abbott. All decorrelation times (measured as e-folding times) fall between 2 and 4 days, for both model and satellite records. Accordingly, the characteristic temporal scales (measured as decorrelation times) of the model calculations agree with those observed from satellites.

[42] Our lag zero squared cross-coherence between temperature and phytoplankton distributions is typically lower by 20 to 30% (satellite values approximately 0.9 versus modeled 0.6 at 50–100 km and 0.5 versus 0.35 at 25–50 km) than that observed by Denman and Abbott (see Figure 9). This may indicate some "mismatch" between modeled temperature variability and modeled phytoplankton variability that is not present in the observations (i.e., in the real world). *Star and Cullen* [1981] explored such mismatches using simple, heuristic models. They noted that something as simple as a non-linear relationship between temperature variations and phytoplankton variations can diminish such correlations below that seen if the variations are linearly related. Coupled biological/physical models are especially sensitive to vertical mixing, and one source of "mismatch"

may be a vertical mixing formulation that introduces a bias into either temperature change or phytoplankton growth as a result of vertical transport [*Durski et al.*, 2004]. This may provide a fruitful area (and a sensible metric) through which to explore various combinations of biological models and vertical mixing schemes.

[43] The success of basic NPZD models, as used in this investigation (and in other studies [e.g., *Spitz et al.* 2003]), suggests that more complicated ecological models may not be necessary for conceptual understanding of simple trophic linkages to circulation. Future models are likely to focus on individual species (or functional groups of species) and specific processes (e.g., harmful algal blooms, multiple nutrient limitation (including iron limitation), or mesozooplankton advection, growth, and behavior). Those efforts must include the complex processes controlling the individual species and specific processes. Nonetheless, those complex formulations will depend upon interactions at lower trophic levels (including photosynthetic processes), and our results imply that bulk pigment distributions can be captured by simple trophic models. Future work comparing the results of our NPZD model to substantially more complicated models would be welcome.

[44] **Acknowledgments.** This is U.S. GLOBEC contribution 279. We are indebted to Kate Hedstrom for her invaluable assistance in configuring and developing the models used here. We also thank Hernan Arango and Alexander Shchepetkin for their extensive contributions to the development of ROMS. We acknowledge two anonymous reviewers for their thoughtful comments. This work was supported by the National Science Foundation through the U.S. GLOBEC Northeast Pacific program (grant OCE 0002893 to principal investigators T. Powell and D. Haidvogel).

References

Abbott, M. R., and P. M. Zion (1985), Satellite observations of phytoplankton variability during an upwelling event, *Cont. Shelf Res.*, *4*, 661–680.

Allen, J. S., and P. A. Newberger (1996), Downwelling circulation on the Oregon continental shelf: Part I. Response to idealized forcing, *J. Phys. Oceanogr.*, *26*, 2011–2035.

Allen, J. S., P. A. Newberger, and J. Federiuk (1995), Upwelling circulation on the Oregon continental shelf: Part I. Response to idealized forcing, *J. Phys. Oceanogr.*, *25*, 1843–1866.

Batchelder, H. P., C. A. Edwards, and T. M. Powell (2002), Individual-based models of copepod populations in coastal upwelling regions: Implications of physiologically and environmentally influenced diel vertical migration on demographic success and nearshore retention, *Prog. Oceanogr.*, *53*, 307–333.

Bendat, J. S., and A. G. Piersol (1986), *Random Data: Analysis and Measurement Procedures*, 2nd ed., John Wiley, Hoboken, N. J.

Bernstein, R. L., L. Breaker, and R. Whritner (1977), California Current eddy formation: Ship, air, and satellite results, *Science*, *195*, 353–359.

Blumberg, A. F., and G. L. Mellor (1983), Diagnostic and prognostic numerical circulation studies of the South Atlantic Bight, *J. Geophys. Res.*, *88*(C8), 4579–4592.

Bond, N. A. (2000), The Pacific Decadal Oscillation, air-sea interaction and central North Pacific winter atmospheric regimes, *Geophys. Res. Lett.*, *27*(5), 731–734.

Bucklin, A. (1991), Population genetic responses of the planktonic copepod *Metridia pacifica* to a coastal eddy in the California Current, *J. Geophys. Res.*, *96*(C8), 14,799–14,808.

Chapman, D. C. (1985), Numerical treatment of cross-shelf open boundaries in a barotropic coastal ocean model, *J. Phys. Oceanogr.*, *15*, 1060–1075.

Chavez, F. P., R. T. Barber, P. M. Kosro, A. Huyer, S. R. Ramp, T. P. Stanton, and B. R. de Mendiola (1991), Horizontal transport and the distribution of nutrients in the coastal transition zone off Northern California: Effects on primary production, phytoplankton biomass and species composition, *J. Geophys. Res.*, *96*(C8), 14,833–14,848.

Chavez, F. P., C. A. Collins, A. Huyer, and D. L. Mackas (2002), Observations of the 1997–98 El Niño along the West Coast of North America, *Prog. Oceanogr.*, *53*, 1–511.

Chavez, F. P., J. Ryan, S. E. Lluch-Cota, and M. C. Ñiquen (2003), From anchovies to sardines and back: Multidecadal change in the Pacific Ocean, *Science*, *299*, 217–221, doi:10.1126/science.1075880.

Curchitser, E., D. Haidvogel, A. Hermann, E. Dobbins, T. Powell, and A. Kaplan (2005), Multi-scale modeling of the North Pacific Ocean: Assessment and analysis of simulated basin-scale variability (1996–2003), *J. Geophys. Res.*, *110*, C11021, doi:10.1029/2005JC002902.

Denman, K. L., and M. Abbott (1988), Time evolution of surface chlorophyll patterns from cross-spectrum analysis of satellite color images, *J. Geophys. Res.*, *93*(C6), 6789–6798.

Denman, K. L., and M. Abbott (1994), Timescales of pattern evolution from cross-spectrum analysis of advanced very high resolution radiometer and coastal zone color scanner imagery, *J. Geophys. Res.*, *99*(C4), 7433–7442.

Denman, K. L., and J. F. Dower (2001), Patch dynamics, in *Encyclopedia of Ocean Sciences*, edited by J. H. Steele, K. K. Turekian, and S. A. Thorpe, pp. 2107–2114, Elsevier, New York.

Denman, K. L., and M. A. Pena (1999), A coupled 1-D biological/physical model of the northeast subarctic Pacific Ocean with iron limitation, *Deep Sea Res., Part II*, *46*, 2877–2908.

Denman, K. L., and T. M. Powell (1984), Effects of physical processes on planktonic ecosystems in the coastal ocean, *Oceanogr. Mar. Biol.*, *22*, 125–168.

Diggle, P. J. (1990), *Time Series: A Biostatistical Introduction*, Oxford Univ. Press, New York.

Durski, S. M., S. M. Glenn, and D. B. Haidvogel (2004), Vertical mixing schemes in the coastal ocean: Comparison of the level 2.5 Mellor-Yamada scheme with an enhanced version of the K profile parameterization, *J. Geophys. Res.*, *109*, C01015, doi:10.1029/2002JC001702.

Edwards, C. A., H. P. Batchelder, and T. M. Powell (2000), Modeling microzooplankton and macrozooplankton dynamics within a coastal upwelling system, *J. Plankton Res.*, *22*, 1619–1648.

Fairall, C. W., E. F. Bradley, J. S. Godfrey, J. B. E. G. A. Wick, and G. S. Young (1996a), Cool-skin and warm-layer effects on sea surface temperature, *J. Geophys. Res.*, *101*(C1), 1295–1308.

Fairall, C. W., E. F. Bradley, D. P. Rogers, J. B. Edson, and G. S. Young (1996b), Bulk parameterization of air-sea fluxes for Tropical Ocean-Global Atmosphere Coupled-Ocean Atmosphere Response Experiment, *J. Geophys. Res.*, *101*(C2), 3747–3764.

Federiuk, J., and J. S. Allen (1995), Upwelling circulation on the Oregon continental shelf: Part II. Simulations and comparisons with observations, *J. Phys. Oceanogr.*, *25*, 1867–1889.

Flather, R. A. (1976), A tidal model of the northwest European continental shelf, *Mem. Soc. R. Sci. Liege*, *6*(10), 141–164.

Gan, J., and J. S. Allen (2002a), A modeling study of shelf circulation off northern California in the region of the coastal ocean dynamics experiment: Response to relaxation of upwelling winds, *J. Geophys. Res.*, *107*(C9), 3123, doi:10.1029/2000JC000768.

Gan, J., and J. S. Allen (2002b), A modeling study of shelf circulation off northern California in the region of the Coastal Ocean Dynamics Experiment: 2. Simulations and comparisons with observations, *J. Geophys. Res.*, *107*(C11), 3184, doi:10.1029/2001JC001190.

Haidvogel, D. B., and A. Beckmann (1999), *Numerical Ocean Modelling*, 330 pp., Imperial Coll. Press, London, UK.

Haidvogel, D. B., H. G. Arango, K. Hedstrom, A. Beckmann, P. Malanotte-Rizzoli, and A. F. Shchepetkin (2000), Model evaluation experiments in the North Atlantic Basin: Simulations in nonlinear terrain-following coordinates, *Dyn. Atmos. Oceans*, *32*, 239–281.

Harding, J., R. Preller, and R. Rhodes (2002), Ocean prediction capabilities (present and future) at the Naval Research Laboratory, in *Oceans '02 MTS/IEEE*, vol. 2, pp. 763–768, Inst. of Electr. and Electron. Eng., New York.

Hermann, A. J., D. B. Haidvogel, E. L. Dobbins, and P. J. Stabeno (2002), Coupling global and regional circulation models in the coastal Gulf of Alaska, *Prog. Oceanogr.*, *53*, 335–367.

Hickey, B. M. (1979), The California Current System: Hypotheses and facts, *Prog. Oceanogr.*, *8*, 191–279.

Hickey, B. M. (1998), Coastal oceanography of western North America from the tip of Baja California to Vancouver Island, in *The Sea*, vol. 11, edited by A. R. Robinson and K. H. Brink, pp. 345–393, John Wiley, Hoboken, N. J.

Hood, R. R., M. R. Abbott, and A. Huyer (1991), Phytoplankton and photosynthetic light response in the coastal transition zone off Northern California in June 1987, *J. Geophys. Res.*, *96*(C8), 14,769–14,780.

Huyer, A. (2003), Preface to special section of enhanced subarctic influence in the California Current, *Geophys. Res. Lett.*, *30*(15), 8019, doi:10.1029/2003GL017724.

Kistler, R., et al. (2001), The NCEP/NCAR 50-year reanalysis: Monthly means CDROM and documentation, *Bull. Am. Meteorol. Soc.*, *82*(2), 247–268.

Levitus, S., and T. P. Boyer (1994), *World Ocean Atlas 1994*, vol. 4, *Temperature*, *NOAA Atlas NESDIS 4*, Natl. Oceanic and Atmos. Admin., Silver Spring, Md.

Levitus, S., R. Burgett, and T. P. Boyer (1994), *World Ocean Atlas 1994*, vol. 3, *Salinity*, *NOAA Atlas NESDIS 3*, Natl. Oceanic and Atmos. Admin., Silver Spring, Md.

Mackas, D. L., L. Washburn, and S. L. Smith (1991), Zooplankton community pattern associated with a California Current cold filament, *J. Geophys. Res.*, *96*(C8), 14,781–14,797.

Mantua, N. J., S. R. Hare, Y. Zhang, J. M. Wallace, and R. C. Francis (1997), A Pacific interdecadal climate oscillation with impacts on salmon production, *Bull. Am. Meteorol. Soc.*, *78*(6), 1069–1079.

Marchesiello, P., J. C. McWilliams, and A. Shchepetkin (2001), Open boundary conditions for long-term integration of regional ocean models, *Ocean Modell.*, *3*, 1–20.

Marchesiello, P., J. C. McWilliams, and A. Shchepetkin (2003), Equilibrium structure and dynamics of the California Current System, *J. Phys. Oceanogr.*, *33*, 753–783.

Martin, A. P. (2003), Phytoplankton patchiness: The role of lateral stirring and mixing, *Prog. Oceanogr.*, *57*, 125–174.

Mellor, G. L., and T. Yamada (1982), Development of a turbulence closure model for geophysical fluid problems, *Rev. Geophys.*, *20*(4), 851–875.

Miller, A. J., et al. (2003), Potential feedbacks between Pacific Ocean ecosystems and interdecadal climate variations, *Bull. Am. Meteorol. Soc.*, *84*(5), 617–633.

Moisan, J. R., and E. E. Hofman (1996a), Modeling nutrient and plankton processes in the California coastal transition zone: 1. A time and depth-dependent model, *J. Geophys. Res.*, *101*(C3), 22,647–22,676.

Moisan, J. R., and E. E. Hofman (1996b), Modeling nutrient and plankton processes in the California coastal transition zone: 3. Lagrangian drifters, *J. Geophys. Res.*, *101*(C3), 22,693–22,704.

Moisan, J. R., E. E. Hofman, and D. B. Haidvogel (1996), Modeling nutrient and plankton processes in the California coastal transition zone: 2. A three-dimensional physical-bio-optical model, *J. Geophys. Res.*, *101*(C3), 22,677–22,691.

National Geophysical Data Center (1988), Digital relief of the surface of the earth, *Data Announce. 88-mgg-02*, Natl. Oceanic and Atmos. Admin., Boulder, Colo.

Newberger, P. A., J. S. Allen, and Y. H. Spitz (2003), Analysis and comparison of three ecosystem models, *J. Geophys. Res.*, *108*(C3), 3061, doi:10.1029/2001JC001182.

Oke, P. R., J. S. Allen, R. N. Miller, and G. D. Egbert (2002a), A modeling study of the three-dimensional continental shelf circulation off Oregon: Part II. Dynamical analysis, *J. Phys. Oceanogr.*, *32*, 1383–1403.

Oke, P. R., J. S. Allen, R. N. Miller, G. D. Egbert, J. A. Austin, J. A. Barth, T. J. Boyd, P. M. Kosro, and M. D. Levine (2002b), A modeling study of the three-dimensional continental shelf circulation off Oregon: Part I. Model-data comparisons, *J. Phys. Oceanogr.*, *32*, 1360–1382.

Oke, P. R., J. S. Allen, R. N. Miller, G. D. Egbert, and P. M. Kosro (2002c), Assimilation of surface velocity data into a primitive equation coastal ocean model, *J. Geophys. Res.*, *107*(C9), 3122, doi:10.1029/2000JC000511.

Pullen, J., and J. S. Allen (2001), Modeling studies of the coastal circulation off northern California: Statistics and patterns of wintertime flow, *J. Geophys. Res.*, *106*(C11), 26,959–26,984.

Richards, F. A. (Ed.) (1981), *Coastal Upwelling*, *Coastal Estuarine Sci.*, vol. 1, edited by F. A. Richards, AGU, Washington D. C.

Shchepetkin, A. F., and J. C. McWilliams (2003), A method for computing horizontal pressure-gradient force in an oceanic model with a nonaligned vertical coordinate, *J. Geophys. Res.*, *108*(C3), 3090, doi:10.1029/2001JC001047.

Smith, S. L., and P. V. Z. Lane (1991), The jet off Point Arena, California: Its role in aspects of secondary production in the copepod *Eucalanus californicus* Johnson, *J. Geophys. Res.*, *96*(C8), 14,849–14,858.

Song, Y. T., and D. Haidvogel (1994), A semi-implicit ocean circulation model using a generalized topography-following coordinate system, *J. Comput. Phys.*, *115*, 228–244.

Spitz, Y. H., P. A. Newberger, and J. S. Allen (2003), Ecosystem response to upwelling off the Oregon Coast: Behavior of three nitrogen-based models, *J. Geophys. Res.*, *108*(C3), 3062, doi:10.1029/2001JC001181.

Star, J. L., and J. J. Cullen (1981), Spectral analysis: A caveat, *Deep Sea Res.*, *28*, 93–97.

Summerhayes, C., , K.-C. Erneis, M. Angel, R. L. Smith, and B. Zeitschel (Eds.) (1995), *Upwelling in the Ocean: Modern Processes and Ancient Records*, John Wiley, Hoboken, N. J.

Thompson, J. D. (1978), The coastal upwelling cycle on a betaplane: Hydrodynamics and thermodynamics, in *Upwelling Ecosystems*, edited by R. Boje and M. Tomczak, pp. 203–222, Springer, New York.

Traganza, E. D., D. A. Nestor, and A. K. McDonald (1980), Satellite observations of a nutrient upwelling off the coast of California, *J. Geophys. Res.*, *85*(4), 4101–4106.

Washburn, L., D. C. Kadko, B. H. Jones, T. Hayward, P. M. Kosro, T. P. Stanton, S. Ramp, and T. Cowles (1991), Water mass subduction and the transport of phytoplankton in a coastal upwelling system, *J. Geophys. Res.*, *96*(C8), 14,927–14,945.

Woodruff, S. D., H. F. Diaz, J. Elms, and S. Worley (1998), COADS Release 2 data and metadata enhancements for improvements of marine surface flux fields, *Phys. Chem. Earth*, *23*, 517–527.

Wroblewski, J. S. (1977), A model of phytoplankon plume formation during variable Oregon upwelling, *J. Mar. Res.*, *35*, 357–394.

E. N. Curchitser, Division of Ocean and Climate Physics, Lamont-Doherty Earth Observatory, Palisades, NY, USA.

E. L. Dobbins and A. J. Hermann, Joint Institute for the Study of Atmosphere and Ocean (JISAO), University of Washington, Seattle, WA, USA.

D. B. Haidvogel, Institute of Marine and Coastal Sciences, Rutgers University, New Brunswick, NJ, USA.

C. V. W. Lewis and T. M. Powell, Department of Integrative Biology, University of California, Berkeley, VLSB Room 5048A, Berkeley, CA 94720, USA. (zackp@berkeley.edu)